Proceedings of *RAGtime 23–25*
Z. Stuchlík, G. Török, V. Karas and D. Lančová, editors, Silesian University in Opava, 2023, pp. 187–198

Nodal precession model applied for twin HF QPOs observed around magnetized neutron stars

Zdeněk Stuchlík[1] and Jaroslav Vrba[1,a]

[1]Research Centre for Theoretical Physics and Astrophysics,
Institute of Physics, Silesian University in Opava,
Bezručovo nám. 13, 746 01 Opava, CZ
[a]Jaroslav.Vrba@physics.slu.cz

ABSTRACT
The nodal oscillations of matter orbiting compact objects such as black holes and neutron stars are usually applied for the explanation of the observed low-frequency quasiperiodic oscillations. In the present paper, we test the applicability of the nodal precession variants of the magnetically modified geodesic model based on the epicyclic motion of slightly charged matter in the magnetosphere of a neutron star represented by the Schwarzschild geometry combined with the dipole magnetic field for fitting of the twin high-frequency quasiperiodic oscillations observed around magnetized neutron stars. We demonstrate that there is a nodal precession variant giving a possibility to fit the data similarly to the standard relativistic precession variant, and we show that the other nodal variant can be clearly excluded.

Keywords: Dipole magnetic field – neutron star – orbiting charged matter – observed quasi-periodic oscillations

1 INTRODUCTION

Charged matter orbiting a magnetized neutron star (NS) can have frequencies of the epicyclic oscillatory motion around equatorial circular orbits, along with the orbital frequency of these circular orbits, comparable to the frequencies of the twin-peak, high-frequency quasiperiodic oscillations (HF QPOs) observed in binary systems containing magnetized NSs (Vrba et al., submitted) – a magnetized NS can be conveniently modeled by the Schwarzschild geometry and the dipole magnetic field that defines the equatorial plane of the whole background. The magnetic parameter b representing the ratio of the electromagnetic and gravitational forces acting on the charged matter must be sufficiently small for comparability to the observed frequencies and can correspond to matter with a very small

978-80-7510-577-6

specific charge so that only charged dust or plasmoids can be considered as acceptable, while protons (electrons) or ions are excluded[1].

In the standard geodesic model of the quasiperiodic oscillations, usually, the relativistic precession variants (or the epicyclic resonance variants) are considered for the explanations of the twin HF QPOs, while the nodal precession frequency is usually applied for an explanation of the low-frequency quasiperiodic oscillations (Tasheva and Stefanov, 2021). Here, we test the possibility of applying the nodal precession variants of the magnetically modified geodesic model, i.e., the variants of the relativistic precession model where the radial epicyclic frequency is substituted by the latitudinal epicyclic frequency, for charged test matter orbiting with epicyclic oscillations a magnetized NS described by the simple model considered in Vrba et al. (submitted).

We give the frequencies of the epicyclic orbital motion of the charged test matter in the equatorial plane of the magnetized NS and present the fitting curves for the nodal precession variants of the magnetically modified geodesic model to the data of the twin HF QPOs observed in binary systems containing NSs. We also give for comparison fitting of these data by the relativistic precession variants of the model.

The radius of the NS is assumed at $R = 3M$, thus, the dipole magnetic field is relevant at the range of $r > 3M$. The epicyclic oscillations around the off-equatorial circular orbits, discussed in detail in Vrba et al. (submitted), are not considered in the present paper, as they predict frequencies higher than the observed frequencies. We focus on the oscillations around the equatorial circular orbits.

Throughout this paper, we use space-like signature $(-+++)$ and a geometric system of units in which $G = c = 1$; we restore them when we need to compare our results with observational data. Greek indices run from $0-3$, and Latin indices run from $1-3$.

2 RELATIVISTIC DIPOLE MAGNETOSPHERE OF NSS

We use the Schwarzschild geometry with line element given in the standard Schwarzschild coordinates (t, r, θ, φ) in the form

$$\mathrm{d}s^2 = -f(r)\,\mathrm{d}t^2 + f(r)^{-1}\,\mathrm{d}r^2 + r^2\left(\mathrm{d}\theta^2 + \sin^2\theta \mathrm{d}\varphi^2\right), \tag{1}$$

where

$$f(r) = 1 - \frac{2M}{r}, \tag{2}$$

M denotes the NS mass.

Around NSs with a dipole magnetic field, the motion of the charged test particles will be limited by their surface. We choose it at $R = 3M$ as this radius is the upper limit on the so-called extremely compact objects having a radius located under the photon sphere of the vacuum Schwarzschild spacetime.

[1] The electromagnetic Lorentz force acting on electrons or protons in the vicinity of black hole event horizon or the NS surface can lead in standard astrophysical situations to the enormous acceleration of electrons, protons, or ions (Stuchlík and Kološ, 2016a; Tursunov et al., 2020a; Stuchlík et al., 2020, 2021).

The dipole magnetic field of a considered NS can be generated by a circular current loop with radius $a \geq 2M$, located on the surface of the NS equatorial plane or by current sheet flashing on the whole NS surface. Using the Schwarzschild metric means that we can approach its horizon, but limits on the radius of realistic NSs have to be taken into consideration. The four-vector electromagnetic potential A^μ of the outer part of the dipole-field solution ($r > a$) in the Schwarzschild metric has only one non-zero component – $A_\mu = (0, 0, 0, A_\varphi)$. The only non-zero component of the four-potential, A_φ, is given by Kovář et al. (2008); Petterson (1974); Preti (2004)

$$\begin{aligned} A_\varphi &= -\mathcal{B}\left[\ln\left(1-\frac{2M}{r}\right)+\frac{2M}{r}\left(1+\frac{M}{r}\right)\right] r^2 \sin^2\theta \\ &= -\mathcal{B}\, h\,(r,\theta) \end{aligned} \tag{3}$$

and the parameter governing the magnetic field is given by

$$\mathcal{B} = \frac{3\mu}{8M^3}, \tag{4}$$

where μ is the magnetic dipole moment of the NS. The Maxwell tensor, $F_{\mu\nu} = A_{\nu,\mu} - A_{\mu,\nu}$, has only two non-zero components

$$\begin{aligned} F_{r\varphi} &= \frac{\partial A_\varphi}{\partial r} = B^\theta \\ &= 2\mathcal{B}\sin^2\theta\left(\frac{2M(r-M)}{2M-r} - r\ln\frac{r-2M}{r}\right) \end{aligned} \tag{5}$$

and

$$\begin{aligned} F_{\theta\varphi} &= \frac{\partial A_\varphi}{\partial \theta} = B^r \\ &= -\mathcal{B}\sin(2\theta)\left[r^2\ln\frac{r-2M}{r} + 2M\,(M+r)\right]. \end{aligned} \tag{6}$$

Clearly, in the equatorial plane, B^r vanishes, while on the symmetry axis also B^θ vanishes.

The magnetic field intensity $B^{\hat{\theta}}$ measured by local static observers on the NS surface enables to express the magnetic dipole moment in the form (Bakala et al., 2010)

$$\mu = \frac{4M^3R^{3/2}\sqrt{R-2M}}{6M\,(R-M) + 3R\,(R-2M)\ln f(R)} B^{\hat{\theta}}. \tag{7}$$

Considering a magnetized NS with $R = 3M$, $M = 2M_\odot$[2] and $B_{\rm surf} = 10^8$ G, we obtain the magnetic dipole moment $\mu \doteq 7 \times 10^{-4}$ m^2.

[2] where $M_\odot$ is the solar mass

3 CHARGED PARTICLE DYNAMICS IN DIPOLE MAGNETIC FIELD OF NSS AND EQUATORIAL CIRCULAR ORBITS

The charged test particle motion is governed by the Lorentz equation

$$\frac{\mathrm{d}u^\mu}{\mathrm{d}\tau} + \Gamma^\mu_{\alpha\beta} u^\alpha u^\beta = \frac{q}{m} F^\mu_\alpha u^\alpha, \tag{8}$$

where u^μ is the four-velocity of the particle with the mass m and charge q, normalized by the condition $u_\alpha u^\alpha = -1$, τ is the proper time of the particle, and $F_{\mu\nu}$ is the antisymmetric tensor of the electromagnetic field. It can be deduced from the Hamiltonian formalism, see e.g. Kološ et al. (2015). The Hamiltonian H reads

$$H = \frac{1}{2} g^{\alpha\beta} (\pi_\alpha - qA_\alpha) \left(\pi_\beta - qA_\beta\right) + \frac{m^2}{2}, \tag{9}$$

where canonical four-momentum π_μ is given by the relation $\pi_\mu = mu_\mu + qA_\mu$. The test particle motion is governed by the Hamilton equations

$$\frac{\mathrm{d}x^\mu}{\mathrm{d}\zeta} = \frac{\partial H}{\partial \pi_\mu}, \quad \frac{\mathrm{d}\pi_\mu}{\mathrm{d}\zeta} = -\frac{\partial H}{\partial x^\mu}, \tag{10}$$

where $\zeta = \tau/m$. The symmetries of the Schwarzschild spacetime (1) and the dipole magnetic field (3) imply the existence of two constants of the particle motion – covariant specific energy and covariant specific axial angular momentum

$$\mathcal{E} = \frac{E}{m} = -\frac{\pi_t}{m} = -g_{tt} u^t, \quad \mathcal{L} = \frac{L}{m} = \frac{\pi_\varphi}{m} = g_{\varphi\varphi} u^\varphi + \bar{q} A_\varphi, \tag{11}$$

where $\bar{q} = q/m$ is the specific charge of the particle. The Hamiltonian (9) can be expressed in the separated form

$$\frac{H}{m^2} = \frac{1}{2} g^{rr} u_r^2 + \frac{1}{2} g^{\theta\theta} u_\theta^2 + \frac{1}{2} g^{tt} \mathcal{E}^2 + \frac{1}{2} g^{\varphi\varphi} \left(\mathcal{L} - \bar{q} A_\varphi\right)^2 + \frac{1}{2} = H_\mathrm{D} + H_\mathrm{P}, \tag{12}$$

consisting of the dynamical, H_D, and potential, H_P, parts

$$H_\mathrm{D} = \frac{1}{2} \left(g^{rr} u_r^2 + g^{\theta\theta} u_\theta^2\right), \tag{13}$$

$$H_\mathrm{P} = \frac{1}{2} \left[g^{tt} \mathcal{E}^2 + g^{\varphi\varphi} \left(\mathcal{L} - \bar{q} A_\varphi\right)^2 + 1\right]. \tag{14}$$

The motion of charged particles can be characterized by the turning points determined by the condition $H_\mathrm{P} = 0$, which gives the regions of the spacetime available (in the $r - \theta$ plane) for the motion of the particles with the given motion constants E, L, in dependence on the electromagnetic interaction given by the particle specific charge and intensity and character of the magnetic field.

3.1 Effective potential and equatorial circular orbits

The motion in the considered background is generally of chaotic character (Stuchlík et al., 2020), but it can be characterized by the effective potential, which represents the barrier

governing the particle motion in dependence on the motion constants and the parameters of the background.

The turning points of the radial motion are determined by the equation $E = V_{\rm eff}(r, \theta; \mathcal{L}, b)$ and the effective potential reads (Kovář et al., 2008)

$$V_{\rm eff}(r,\theta) \equiv -g_{tt}\left[g^{\varphi\varphi}\left(\mathcal{L} - \bar{q}A_\varphi\right)^2 + 1\right] = \left(1 - \frac{2M}{r}\right)\left[\left(\frac{\mathcal{L}}{r\sin\theta} - b\,h\,(r,\theta)\; r\sin\theta\right)^2 + 1\right], \tag{15}$$

being thus given by the motion constant $\mathcal{L}$ and the "magnetic parameter" b determining the intensity of the particle interaction with the given magnetic field

$$b = \bar{q}\mathcal{B} = \frac{q}{m}\frac{3\mu}{8M^3}. \tag{16}$$

The positive (negative) value of the magnetic parameter b corresponds to the magnetic attraction (repulsion) with inward (outward) directed electromagnetic Lorentz force.

The local extrema of the effective potential determines the circular orbits of charged particles that are stable (unstable) for local minima (maxima). The epicyclic motion is possible only around the stable circular orbits. Here, we concentrate on the equatorial circular orbits that must be considered in the regions where stability is satisfied for both radial and latitudinal (vertical) perturbations – for details, see Vrba et al. (submitted). The axial angular momentum $\mathcal{L}$ of the charged particles following the equatorial circular orbits with fixed parameter b are given by the relations (assuming in the following $M = 1$)

$$\mathcal{L}_{\rm c} = \frac{b}{r-3}\left[r^2\,{\rm Ln}\,(r) + 2r + 6\right] + r\frac{\triangle(r,b)}{r-3}, \tag{17}$$

where $\triangle(r,b) = \sqrt{b^2\left[2\,(r-1) + (r-2)\,r\,{\rm Ln}\,(r)\right]^2 + r - 3}$ and ${\rm Ln}\,(r) = \ln\frac{r-2}{r}$. The specific energy $\mathcal{E}$ of the particles at these circular orbits reads

$$\mathcal{E}_{\rm c} = r^{-1}\sqrt{1 - \frac{2}{r}}\left\{-br^2 + \left[r\frac{\triangle(r,b)}{r-3} + \frac{br^2\,{\rm Ln}\,(r) + 2br + 6b}{r-3} - r^2\,{\rm Ln}\,(r) - 2\,(r+1)\right]^2\right\}^{\frac{1}{2}}. \tag{18}$$

Because of the symmetry of the effective potential relative to the sign change of $\mathcal{L}$ and b, we can restrict attention to the corotating orbits. We can see that the circular orbits can exist at $r > 3$, while both the specific angular momentum and specific energy diverge if $r \to 3$; at $r = 3$, the equatorial photon circular orbit is located. The special reality condition

$$\left[2b\,(r-1) + b\,(r-2)\,r\,{\rm Ln}\,(r)\right]^2 + r - 3 \geq 0, \tag{19}$$

governing the existence of the equatorial circular orbits at the radii $2 < r < 3$ is irrelevant here, as we assume $R = 3$.

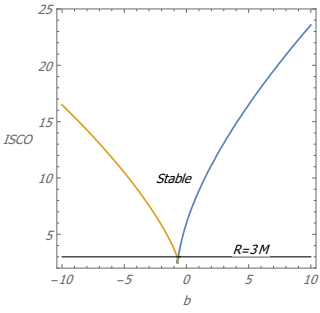

Figure 1. Dependence of ISCO position on the dipole magnetic field parameter b. The blue curve gives ISCO due to instability in the radial direction, and the orange curve gives ISCO due to instability in the latitudinal direction – relating to the off-equatorial circular orbits (Vrba et al., submitted).

The stability of the equatorial circular orbits in both radial and latitudinal directions is studied in detail in Vrba et al. (submitted) and we simply use the results of this paper, see Figure 1. We give only short summary of these results: for values of the magnetic parameter $b > b_{\mathrm{rISCO}}(r = 3) \doteq -0.654$ a marginally stable circular orbit exists at some $r > 3$ due to instability in the radial direction, while for values of $b < b_{\theta\mathrm{ISCO}}(r = 3) \doteq -0.751$, the instability at the marginally stable orbit is in the latitudinal direction – two fundamentally distinct scenarios of the instability of the equatorial circular orbits arise; in the case of $b_{\theta\mathrm{ISCO}}(r = 3) \doteq -0.751 < b < b_{\mathrm{rISCO}}(r = 3) \doteq -0.654$, the equatorial circular orbits are stable at $r > 3$ (Vrba et al., submitted).

4 FREQUENCIES OF THE EPICYCLIC EQUATORIAL ORBITAL MOTION

The locally measured epicyclic frequencies around the equatorial circular orbits are given in general axially symmetric backgrounds of the type considered here by Kološ et al. (2015)

$$\omega_{\mathrm{r}}^2(r) = \partial_{rr}^2 V_{\mathrm{eff}}, \qquad \omega_{\theta}^2(r) = \partial_{\theta\theta}^2 V_{\mathrm{eff}}. \tag{20}$$

The orbital frequency of the circular orbit related to the particle's proper time reads

$$\omega_{\varphi} = \frac{\mathrm{d}\varphi}{\mathrm{d}\tau} = \mathcal{L}(r, \theta = \pi/2)\, g^{\varphi\varphi} - bh(r, \theta = \pi/2)\,. \tag{21}$$

Since the frequencies (20) are calculated for the local comoving observer, we have to transform to the system of a static observer at infinity due to the redshift effect, using the standard SI units. The transformation for general locally measured angular frequency ω to general frequency ν measured by the distant observer can be expressed in the form

$$\nu_i = \frac{1}{2\pi}\frac{c^3}{GM}\frac{\omega_i}{-g^{tt}\mathcal{E}(r)}, \tag{22}$$

where $i = \{r, \theta, \varphi\}$.

By using the effective potential introduced above (20), we can derive the expressions for the local epicyclic frequencies of charged particles in the field of a magnetized NS with magnetic dipole field in the form (Vrba et al., submitted)

$$\omega_{\mathrm{r}}^2 = -\frac{1}{r^5\,(r-2)^2}\times$$
$$\left\{b^2(r-2)\left[(r-2)^2\,r^4\mathrm{Ln}^2\,(r)+4\,(r-3)\,r^4\,\mathrm{Ln}\,(r)+4\left(r^4-2r^3-3r^2-4r+12\right)\right]\right.$$
$$+\frac{3\,(r-2)^3\left[r\triangle(r,b)+br^2\,\mathrm{Ln}\,(r)+2br+6b\right]^2}{(r-3)^2}-2\,(r-2)\,r^3$$
$$-\frac{16b\left(2r^2-7r+6\right)\left[r\triangle(r,b)+br^2\,\mathrm{Ln}\,(r)+2br+6b\right]}{r-3}$$
$$\left.-2\,(r-2)\,r^3\,\frac{\left[\triangle(r,b)+br^2\,\mathrm{Ln}\,(r)+2br-2br\,\mathrm{Ln}\,(r)-2b\right]^2}{(r-3)^2}\right\}, \tag{23}$$

$$\omega_\theta^2 = \frac{1}{r^4}\left\{\frac{\left(r\triangle(r,b)+br^2\,\mathrm{Ln}\,(r)+2br+6b\right)^2}{(r-3)^2}\right.$$
$$\left.-b^2r^4\mathrm{Ln}^2\,(r)-4b^2r^3\,\mathrm{Ln}\,(r)-4b^2r^2-4b^2r^2\,\mathrm{Ln}\,(r)-8b^2r-4b^2\right\}, \tag{24}$$

$$\omega_\varphi = \frac{\triangle(r,b)+br^2\,\mathrm{Ln}\,(r)+2br-2br\,\mathrm{Ln}\,(r)-2b}{(r-3)\,r}. \tag{25}$$

See also Bakala et al. (2010), where the frequencies were derived in different ways, having the same form. For a slowly rotating sphere, the frequencies were derived in Bakala et al. (2012). By applying transformation (22) to equations (23-25), we obtain the observable epicyclic frequencies. The behavior of the frequencies $\nu_r\,(r)$, $\nu_\theta\,(r)$ and $\nu_\varphi\,(r)$, as functions of the radial coordinate r in equatorial plane ($\theta = \pi/2$), is demonstrated in Figure 2.

The frequencies of epicyclic oscillations of charged particles in the field of a NS with a magnetic dipole differ in many aspects from the frequencies of uncharged particles in a Schwarzschild compact object. The most remarkable manifestation of these differences is the separation of the latitudinal and Keplerian frequencies. This occurs in the presence of any nonzero magnetic field in the case of a homogeneous magnetic field, it was studied in (in the case of a homogeneous magnetic field, it was studied in Kološ et al., 2015) and is a consequence of the disruption of spherical symmetry of the background. The strong differences in behavior of the epicyclic and orbital frequencies demonstrated in the case of the dipole magnetic field inspired the idea to apply the nodal precession variants of the magnetically modified geodesic model to the case of HF QPOs observed in the binary systems containing a NS.

Another effect that influences the behavior of the epicyclic motion is the shift in the location of the ISCO in dependence on the parameter b (see Figure 1). The last significant difference is the interchange of the profiles of the epicyclic latitudinal and radial frequencies for negative values of the parameter b due to the θ-instability – see Figure 2.

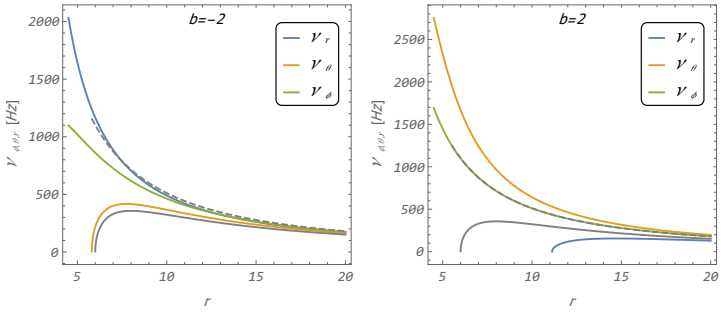

Figure 2. Epicyclic frequencies in the equatorial plane ($\theta = \pi/2$) for a NS with mass $M = 2M_\odot$ and various strengths of dipole magnetic field constructed for frequencies of the epicyclic equatorial circular motion. The colored curves represent the epicyclic frequencies in the dipole configuration. The solid black and dashed black curves represent the radial and latitudinal (Keplerian) frequencies in the Schwarzschild case, respectively.

5 FITTING TO THE HF QPOS

The HF QPOs play a crucial role in astrophysics as they provide a very solid basis for predicting the parameters of compact objects in accretion systems.

5.1 Geodesic models and their modifications

There are two main variants (and their subvariants) of the so-called geodesic model of HF QPOs using the frequencies of the epicyclic oscillations and the orbital motion in fitting the data observed in the astrophysical systems containing a black hole or a NS (Stuchlík and Kološ, 2016b): the Epicyclic Resonance (ER) model (Kluzniak and Abramowicz, 2001; Abramowicz and Kluźniak, 2001; Remillard and McClintock, 2006; Török et al., 2005) and the Relativistic Precession (RP) model (Stella et al., 1999a,b). For details of the geodesic model of HF QPOs and their applications on the situations around BHs and NSs, see Stuchlík et al. (2013); Stuchlík and Kološ (2016b).

Modification of the variants of the geodesic model by the presence of a magnetic field acting on a slightly charged orbiting matter significantly enlarges the ability of the modified model to fit the observational data because of adding a new free parameter b reflecting the electromagnetic interaction of the charged matter with the external magnetic field (Bakala et al., 2010; Kološ et al., 2017; Stuchlík et al., 2022). Here, we test in a rough way the applicability of the new variant, called nodal precession and representing a direct modification of the relativistic precession variant by substituting the radial epicyclic frequency with the latitudinal epicyclic frequency to fit the data of HF QPOs. In order to estimate the efficiency of the possibility of fitting, we compare the fitting curves of the whole set of the NS HF QPO data for the nodal precession and relativistic precession variant of the magnetically modified geodesic model.

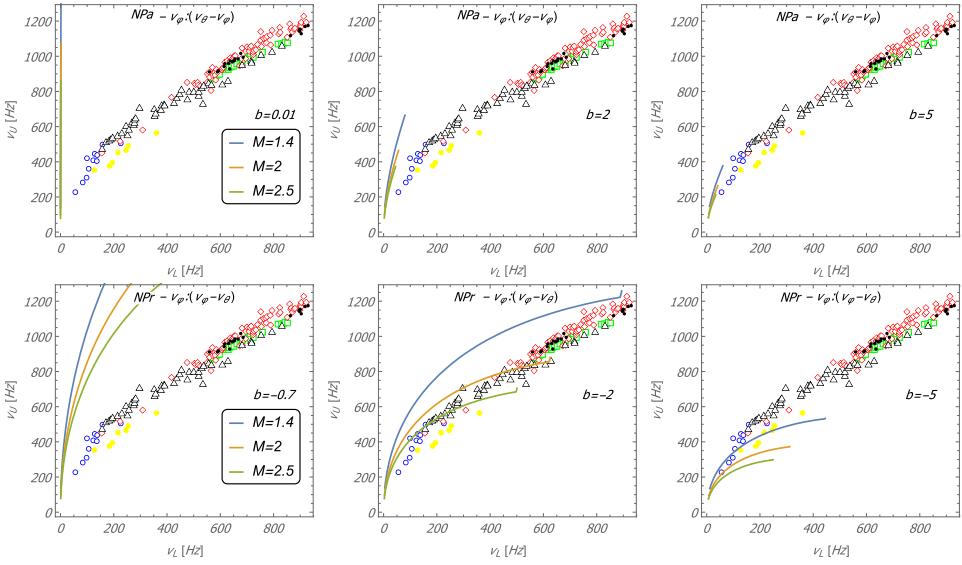

Figure 3. The NP variants of the equatorial geodesic model. HF QPOs fits for the collected data of selected sources. We variate dipole magnetic parameter b and mass of the NS.

We present only rough estimates of possible fitting to the HF QPOs observed in binary systems containing NSs using the collected data of the observed binary systems. Detailed fitting to data from individual sources is planned for future papers.

We thus use the upper ($\nu_{\rm U}$) and lower ($\nu_{\rm L}$) frequencies of the two peaks observed in the data, which are as follows for each model. The variants must differ for $b > 0$ and $b < 0$ due to the different radial profiles of the frequencies ν_r, ν_θ, ν_φ

$\underline{\rm NP_a}$: $\nu_{\rm U} = \nu_\varphi$ and $\nu_{\rm L} = \nu_\theta - \nu_\varphi$

$\underline{\rm RP_a}$: $\nu_{\rm U} = \nu_\varphi$ and $\nu_{\rm L} = \nu_\varphi - \nu_r$

$\underline{\rm NP_r}$: $\nu_{\rm U} = \nu_\varphi$ and $\nu_{\rm L} = \nu_\varphi - \nu_\theta$

$\underline{\rm RP_r}$: $\nu_{\rm U} = \nu_\varphi$ and $\nu_{\rm L} = \nu_r - \nu_\varphi$.

The fitting of the upper and lower frequency curves for each model to the astrophysical data are shown in Figure 4, where is presented the NP variants, while Figure 3 corresponds to the RP variants. It is evident that in one of the sub-variants, both the NP and RP are promising, while the other seems to be quite excluded. It is evident that both models show quite promising results for the specifically chosen values of parameter b. The RP model exhibits the best agreement with astrophysical data for low positive values $b \sim 0.01$, whereas the NP model shows the most promising results around negative values $b \sim -2$.

The charged particle within our test particle model can also represent an elementary particle (electron, proton), but the fitting to HF QPO data cannot be fulfilled for $B = 10^8 - 10^{12}$ G in strong NS magnetosphere. Our "charged test particle" more likely represents a hot spot (plasmoid, "ball lightning") in accretion flow with density lower (higher) than the surrounding plasma and with accumulated net electric charge (Ripperda et al.,

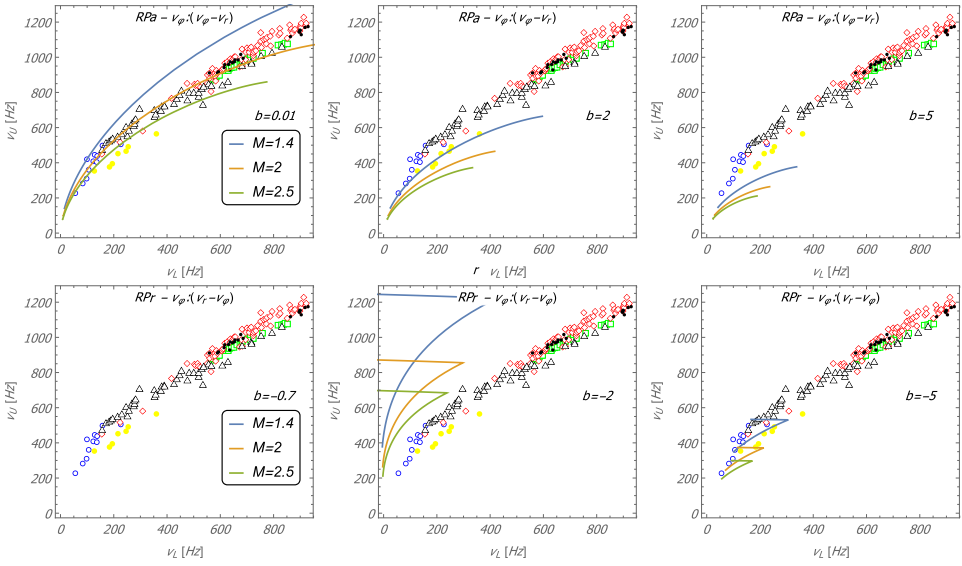

Figure 4. The RP variants of the equatorial geodesic model. HF QPOs fits for the collected data of selected sources. We variate dipole magnetic parameter b and mass of the NS.

2020; Tursunov et al., 2020b). Our HF QPOs fits can be thus used for estimates of such hot-spot (plasmoid) net specific charge. Another possible application of our "charged particle" model is that it could model magnetic field influence on quasi-neutral plasma flow. Such a connection between charged particle dynamics and plasma flow is based on the interesting finding that the fundamental frequencies of test particle dynamics could be present in the spectra of oscillating accretion disk (Mishra et al., 2019).

6 CONCLUSIONS

The presence of magnetic fields around NS is of utmost importance in numerous astrophysical contexts, as their effects can be of critical significance, even in the case of electromagnetic interaction, which is small in comparison with gravitational interaction. In fitting to data of HF QPOs from the atol sources containing NSs, the magnetically modified variants of the geodesic model based on epicyclic oscillations of orbiting charged matter can be promising. We have shown that not only the $\mathrm{PR_a}$ variant reflecting Lorentz attraction can give fits for $b \sim 0.01$, but also the $\mathrm{NP_r}$ variant with Lorentz repulsion can allow good fits for $b \sim -2$.

The fitting of the HF QPOs should be thus to slightly charged matter, e.g. to charged dust, plasmoids, or structures similar to ball lighting, if we consider the realistic magnetic field as observed in the atoll sources having NSs with magnetic field intensity ranging from 10^8G to 10^{12} G. For example, singly ionized dust grains with masses of the order of 10^{-13} g for $b \sim 0.01$ (10^{-11} g for $b \sim -2$) could be the potential contributors to this phenomenon, for

the magnetic field strengths of $B = 10^{10}$ G. We can expect that the two discussed variants of the magnetically modified geodesic model of HF QPOs could improve precession of the individual data fits in some of the observed binaries containing NSs. Further improvement could be expected with the inclusion of the rotational effect of the NS that can be realized at least on the level of the Lense-Thirring term to the Schwarzschild geometry.

ACKNOWLEDGEMENTS

The authors would like to acknowledge the institutional support of the Research Centre For Theoretical Physics and Astrophysics, Institute of Physics, Silesian University in Opava.

REFERENCES

Abramowicz, M. A. and Kluźniak, W. (2001), A precise determination of black hole spin in GRO J1655-40, *Astronomy and Astrophysics*, **374**, pp. L19–L20, arXiv: astro-ph/0105077.

Bakala, P., Urbanec, M., Šrámková, E., Stuchlík, Z. and Török, G. (2012), On magnetic-field-induced corrections to the orbital and epicyclic frequencies: paper II. Slowly rotating magnetized neutron stars, *Classical and Quantum Gravity*, **29**(6), 065012.

Bakala, P., Šrámková, E., Stuchlík, Z. and Török, G. (2010), On magnetic-field-induced non-geodesic corrections to relativistic orbital and epicyclic frequencies, *Classical and Quantum Gravity*, **27**(4), 045001.

Kluzniak, W. and Abramowicz, M. A. (2001), Strong-Field Gravity and Orbital Resonance in Black Holes and Neutron Stars — kHz Quasi-Periodic Oscillations (QPO), *Acta Physica Polonica B*, **32**(11), p. 3605.

Kološ, M., Stuchlík, Z. and Tursunov, A. (2015), Quasi-harmonic oscillatory motion of charged particles around a Schwarzschild black hole immersed in a uniform magnetic field, *Classical and Quantum Gravity*, **32**(16), 165009, arXiv: 1506.06799.

Kološ, M., Tursunov, A. and Stuchlík, Z. (2017), Possible signature of the magnetic fields related to quasi-periodic oscillations observed in microquasars, *European Physical Journal C*, **77**(12), 860, arXiv: 1707.02224.

Kovář, J., Stuchlík, Z. and Karas, V. (2008), Off-equatorial orbits in strong gravitational fields near compact objects, *Classical and Quantum Gravity*, **25**(9), 095011, arXiv: 0803.3155.

Mishra, B., Kluźniak, W. and Fragile, P. C. (2019), Breathing Oscillations in a Global Simulation of a Thin Accretion Disk, *Monthly Notices of the RAS*, **483**(4), pp. 4811–4819, arXiv: 1810.05755.

Petterson, J. A. (1974), Magnetic field of a current loop around a Schwarzschild black hole, *Physical Review D*, **10**(10), pp. 3166–3170.

Preti, G. (2004), On charged particle orbits in dipole magnetic fields around Schwarzschild black holes, *Classical and Quantum Gravity*, **21**(14), pp. 3433–3445.

Remillard, R. A. and McClintock, J. E. (2006), X-Ray Properties of Black-Hole Binaries, *Annual Review of Astronomy & Astrophysics*, **44**(1), pp. 49–92, arXiv: astro-ph/0606352.

Ripperda, B., Bacchini, F. and Philippov, A. A. (2020), Magnetic Reconnection and Hot Spot Formation in Black Hole Accretion Disks, *Astrophysical Journal*, **900**(2), 100, arXiv: 2003.04330.

Stella, L., Vietri, M. and Morsink, S. M. (1999a), Correlations in the Quasi-periodic Oscillation Frequencies of Low-Mass X-Ray Binaries and the Relativistic Precession Model, *Astrophysical Journal Letters*, **524**(1), pp. L63–L66, arXiv: astro-ph/9907346.

Stella, L., Vietri, M. and Morsink, S. M. (1999b), Correlations in the Quasi-periodic Oscillation Frequencies of Low-Mass X-Ray Binaries and the Relativistic Precession Model, *Astrophysical Journal Letters*, **524**(1), pp. L63–L66, arXiv: astro-ph/9907346.

Stuchlík, Z. and Kološ, M. (2016a), Acceleration of the charged particles due to chaotic scattering in the combined black hole gravitational field and asymptotically uniform magnetic field, *European Physical Journal C*, **76**, 32, arXiv: 1511.02936.

Stuchlík, Z. and Kološ, M. (2016b), Models of quasi-periodic oscillations related to mass and spin of the GRO J1655-40 black hole, *Astronomy and Astrophysics*, **586**, A130, arXiv: 1603.07366.

Stuchlík, Z., Kološ, M., Kovář, J., Slaný, P. and Tursunov, A. (2020), Influence of Cosmic Repulsion and Magnetic Fields on Accretion Disks Rotating around Kerr Black Holes, *Universe*, **6**(2), p. 26.

Stuchlík, Z., Kološ, M. and Tursunov, A. (2021), Penrose Process: Its Variants and Astrophysical Applications, *Universe*, **7**(11), p. 416.

Stuchlík, Z., Kološ, M. and Tursunov, A. (2022), Large-scale magnetic fields enabling fitting of the high-frequency QPOs observed around supermassive black holes, *Publications of the Astronomical Society of Japan*, **74**(5), pp. 1220–1233.

Stuchlík, Z., Kotrlová, A. and Török, G. (2013), Multi-resonance orbital model of high-frequency quasi-periodic oscillations: possible high-precision determination of black hole and neutron star spin, *Astronomy and Astrophysics*, **552**, A10, arXiv: 1305.3552.

Tasheva, R. and Stefanov, I. (2021), Geodesic model complience with the frequencies of the observed X-ray quasi-period oscillations of XTE J1807-294, *Bulgarian Astronomical Journal*, **34**, p. 103, arXiv: 2305.12198.

Török, G., Abramowicz, M. A., Kluźniak, W. and Stuchlík, Z. (2005), The orbital resonance model for twin peak kHz quasi periodic oscillations in microquasars, *Astronomy and Astrophysics*, **436**(1), pp. 1–8.

Tursunov, A., Stuchlík, Z., Kološ, M., Dadhich, N. and Ahmedov, B. (2020a), Supermassive Black Holes as Possible Sources of Ultrahigh-energy Cosmic Rays, *Astrophysical Journal*, **895**(1), 14, arXiv: 2004.07907.

Tursunov, A., Zajaček, M., Eckart, A., Kološ, M., Britzen, S., Stuchlík, Z., Czerny, B. and Karas, V. (2020b), Effect of Electromagnetic Interaction on Galactic Center Flare Components, *Astrophysical Journal*, **897**(1), 99, arXiv: 1912.08174.

Vrba, J., Kološ, M. and Stuchlík, Z. (submitted), Charged particles in dipole magnetosphere of neutron stars: epicyclic oscillations in and off equatorial plane.